

Article citation info:

Janutėnienė J, Bogdevičius M, Jankūnas V, Janutėnaitė-Bogdaniienė J, Andziulis A, Kurmis M, Drungilas D. Investigation of dynamics and power needs for container unloading from ship process. *Eksploatacja i Niezawodność – Maintenance and Reliability* 2022; 24 (1): 89–99, <http://doi.org/10.17531/ein.2022.1.11>.

## Investigation of dynamics and power needs for container unloading from ship process

Indexed by:



Jolanta Janutėnienė<sup>a</sup>, Marijonas Bogdevičius<sup>b</sup>, Valdas Jankūnas<sup>a</sup>, Jūratė Janutėnaitė-Bogdaniienė<sup>c,\*</sup>,  
Arūnas Andziulis<sup>a</sup>, Mindaugas Kurmis<sup>a</sup>, Darius Drungilas<sup>a</sup>

<sup>a</sup>Klaipėda University, Faculty of Marine Technologies and Natural Science, Bijunu str. 17, LT-91225 Klaipėda, Lithuania

<sup>b</sup>Vilnius Gediminas Technical University, Faculty of Transport Engineering, Saulėtekio al. 11, LT-10223 Vilnius, Lithuania

<sup>c</sup>Vilnius Gediminas Technical University, Faculty of Fundamental Sciences, Saulėtekio al. 11, LT-10223 Vilnius, Lithuania

### Highlights

- A complex mathematical model describes the process of container lifting from a ship.
- The power of frictional forces between oscillating ship and container were analyzed.
- Lifting power needs dependency on mass of container and frictional forces was deduced.
- Results can be applied to safety and efficient handling of containers in green ports.

### Abstract

The operational problem of container unloading from the ship is analyzed in this paper. Dynamic “crane-cargo-ship” system was investigated, and a mathematical model was created. In the model, the gap between the container and the ship’s cargo hold, the mass of the cargo, the container’s center of the mass, and the frictional forces that may occur during lifting from the cargo hold were estimated. Numerical analysis of the system was performed. Results of numerical analysis were compared with experimental measurements of containers unloading process in port. Requirement of lifting power was modelled depending on mass of cargo. Additional power needs in case of contact forces between container and wall of the ship’s cargo hold were calculated. Rational lifting conditions could be deduced using a created mathematical model and the reliability of the container and cargo during lifting could be deduced.

### Keywords

This is an open access article under the CC BY license (<https://creativecommons.org/licenses/by/4.0/>)

container unloading, mathematical modelling, numerical analysis, port, ship, ship’s cargo hold.

## 1. Introduction

Container handling in world ports has increased significantly over the last decade. This has caused both technical and environmental problems in ports, increased the need to automate loading processes, their safety and at the same time reduce energy consumption and pollution. Maritime transport makes up 3% of all CO<sub>2</sub> emissions and various possible solutions on how to reduce it were proposed in paper [4]. A thorough analysis of 150 articles presented by authors shows that one way to address the problem is by evaluating ship efficiency, greenhouse gases (GHG) emissions from shipping, ship design, operations, or performance. Authors of the works [4] divided six main groups (hull design, economy of scale, power and propulsion, speed, alternative sources, weather routing and scheduling) where improvements can lead to reduced (GHG). Another approach to reduce emissions that are generated by maritime transport - green ports. About 85% of all emissions in ports come from container ships and tankers. Ports suffer not only from GHG but also from external costs that are caused by shipping emissions which affect the local population [14]. Although reduced emissions in ports will not have such a major impact on emissions worldwide, it is still a necessary and significant

problem that must be addressed [9]. ESPO Green guide was presented in 2021 which provides an extensive database of good green practices in European ports. The aim is to reduce environmental impacts of the port area, greening of the port area, communicating to enhance common understanding, increasing transparency, etc. A guide provides target dates, expected results, and steps that should be taken to achieve the goals.

Container cranes are widely used equipment especially in ports for cargo movement. The main requirements for quay cranes are as follows: the ability to lift the selected maximum load weight; high structural stiffness; high speed; reliable and safe work, etc. Efficiency of container cranes is determined by various parameters, mainly by their speed and energy consumption. A strategy of port (GHG) Emissions Reduction is presented in the article [2]. Authors analyzed 159 academic peer-reviewed studies and provided structured data. The analysis of shipping and land transport (trucks) showed that ports can make a huge impact in reducing total GHG emission and improving energy consumption efficiency [2]. Emission assessment and energy consumption of ports was analyzed in an article [5]. The research showed that efficiency of energy consumption can reach up to 90%. However, there is no single common method for all the ports. Thus, each port

(\*) Corresponding author.

E-mail addresses: J. Janutėnienė (ORCID: 0000-0002-5612-4737): [jolanta.januteniene@ku.lt](mailto:jolanta.januteniene@ku.lt), M. Bogdevičius (ORCID: 0000-0003-4947-7638): [marijonas.bogdevicius@vilniustech.lt](mailto:marijonas.bogdevicius@vilniustech.lt), V. Jankūnas (ORCID: 0000-0003-3077-3568): [valdas.jankunas@ku.lt](mailto:valdas.jankunas@ku.lt), J. Janutėnaitė-Bogdaniienė (ORCID: 0000-0002-1065-7095): [j.janutenaitė-bogdaniene@vilniustech.lt](mailto:j.janutenaitė-bogdaniene@vilniustech.lt), A. Andziulis (ORCID: 0000-0002-1735-8901): [arunas.andziulis@ku.lt](mailto:arunas.andziulis@ku.lt), M. Kurmis (ORCID: 0000-0002-4787-9791): [Mindaugas.kurmis@ku.lt](mailto:Mindaugas.kurmis@ku.lt), D. Drungilas (ORCID: 0000-0002-7821-3183): [darius.drungilas@ku.lt](mailto:darius.drungilas@ku.lt)

should perform a thorough economical, technical, and environmental evaluation before implementing energy and pollution reduction measures. GHG reduction can be achieved not only by switching to renewable energy sources, but by saving energy, improving processes so that energy consumption would be more efficient.

A power consumption problem was addressed in previous research where the cargo lowering process of a quay crane was analyzed [8]. Simulation and real experiments have shown that it is possible to ensure a more time efficient and thus energy efficient process. Many risks arise during the container handling procedures performed by the quay cranes and operators. A novel container transportation security and cargo safety assurance method was developed in paper [11]. Such results led to further research and optimization of the cargo lifting process from the ship.

## 2. Container crane operation and process optimization. A literature review

Port cranes are subjected to various external disturbances which affect operational efficiency. One of such disturbances is the wind and wind loads can lead to large amplitude oscillations of the container or crane itself thus having a negative impact to the whole efficiency of the system. A three-dimensional modeling of container cranes subject to wind loads is presented in the work [3]. Inclination and inextensibility of cables were analyzed in the paper [10]. Main five parameters of crane were taken into account (container mass, frictions at bridge motion, trolley movement handling rope, hydraulic cylinder absorptions) and wind distribution parameters ( $w_x$ ,  $w_y$ ,  $w_\phi$ , and  $w_\theta$ ) were approximated. Novel control algorithm was created, it takes into account fractional-order calculus, sliding mode and adaptive control thus enabling a more precise whole crane control. A similar problem for a 3D overhead crane with simultaneous payload hoisting and wind disturbances was analyzed in the paper [1]. The authors have presented an adaptive command shaping (ACS) technique combined with an integral sliding mode (ISM) control. The ACS is responsible for unwanted payload sway control and hoisting minimization, whereas ISM control is for disturbance compensation. Simulation and experiment with different cable lengths and payload hoisting showed that a combination of ACS and ISM control resulted in significant reduction of payload sway thus ensuring a more accurate precision [1]. When investigating the whole container loading/unloading system, it is important to consider moving load problems as bending stresses are affected by multiple factors such as inertial forces, flexibility of the system, swing angle, etc., especially when bigger mass ratios are taken into consideration [15]. Ship based crane payload motion was investigated in the paper [22]. Stochastic dynamics, stability and control dynamics were separated as the main factors. Coupled simulation of crane operation and ship response in waves is presented in work [6]. Equations of kinematics and dynamics of the system were written. A digital twin of the ship with a crane was created which allows analysis of the dynamics of the full system. Most crane systems exhibit double pendulum characteristics that lead to a difficult control of the whole process. Due to complexity of the analyzed problem, a quadratic programming (QP) based energy-optimal solution with certain constraints for velocity, acceleration and amplitudes of the angle swings was formulated and an energy-optimal trajectory planner was presented with satisfactory results [18]. A research of double pendulum crane system with distributed mass beam showed that by applying sliding mode control allows to stabilize a system [20] and then adding a low-pass filter to the previously developed time optimal anti

swing controller could reduce the residual oscillation angle of the distributed mass beams (DMB) [21]. Velocity and displacement control was taken as the basis for the sliding mode control utilizing a low-pass filter to achieve the minimum maximum residual angle.

A different approach to the energy saving problem is to try to recover the energy consumed during the operation of the crane. Operation data of a rubber tire gantry (RTG) crane was collected and energy consumption by various motors analyzed in the paper [16]. For this rectifier energy, hoist energy, gantry energy, losses were calculated, and potentially recoverable energy estimated. The results showed that it is possible to recover about half of the energy consumed during the crane operation. Energy consumption by adding components to a standard query crane that improve cycle times could be saved is presented in paper [17]. Two types of advanced query cranes were presented, and their cycle times calculated. The results showed a significant increase in productivity compared to a common query crane. Power demand can be controlled starting from early stages of crane design thus ensuring reduced dynamic overload values [7]. The analyzed crane is subjected to loads as lifting load, counterweight and weight of the jib and forces acting in ropes during the lift. Energy consumption as a function of the mass of the transported mass was investigated in the article [13]. A mathematical model of a forest crane for the analysis of its operating cycle dynamics is presented in the work [19]. Second-order LaGrange equations are used to derive equations of motion. In the mathematical model, the frictional forces are evaluated. The results of numerical analysis confirm that friction can have a significant impact and could be considered in the initial phase at crane design. Analysis of the lifting mechanism for various lifting cases is presented in paper [12]. The influence of start-up time on machine overloads and energy overloads was determined. Influence of lifting height and lifting weight on the drive overload and energy consumption was presented.

A dynamic system “Crane-Cargo-Ship” is analyzed in this paper. Dynamic model of the crane consists of an electric motor, gearbox and drum, rope system, container, and the spreader of the crane. Mathematical model was created which describes the dynamic process when a container is lifted from the ship’s cargo hold. Parameters such as a gap between container and cargo hold, cargo weight, mass center of containers, frictional forces that may occur during lifting from the cargo hold are taken into a mathematical model. Results of experimental measurements of the container unloading process are used for verification of mathematical models.

Main aim of this paper is to analyze conditions of container unloading from ship when ship oscillates, and friction forces arise between container and ship hold; to deduce unloading duration and power need depending on container masses and friction forces.

Based on the developed mathematical model of the “Crane-Cargo-Ship” system, it is possible to analyze the lifting dynamics and assess the problems of cargo reliability.

Steps of investigation of the “Crane-Cargo-Ship” system are as follows: creation of dynamical model; creation of mathematical model; analysis of experimental measurements of container unloading from the ship; creation of programming code; numerical analysis and comparison with experimental results.

## 3. Mathematical model of container handling process “Crane-Cargo-Ship”

### 3.1. Crane transmission mathematical model

Table 1. Symbols and descriptions

Symbol	Units	Description
$r_2 \dots r_9$	m	Radiuses of gearbox

$u_R$	m	Gear ratio of transmission
....	rad	Angles of rotation of rotor and gears
$\varphi_{10}$	rad	Angle of rotation of drum
$\varphi_{12} \dots \varphi_{17}$	rad	Angles of rotation of pulleys
$M_{eng}$	Nm	Torque moment of the asynchronous electric motor
$\omega_0$	Nm	Synchronous angular velocity of motor
$c_v, d_v$	Nm, 1/s	Parameters of the electric motor
$F_{O10XLR}, F_{O10ZRL}$	N	Reaction forces in the right and left supports of drum
$F_N$	N	Normal force in support of drum
$k_{SUPP}$	N/m	Contact stiffness coefficient
$\delta_N$	m	Penetration shaft of drum
$D$	-	Coefficient which evaluates hysteresis of contact force
$\delta_{N\_max}$	m/s	Maximal values of velocity of penetration
$e_{RES}$	-	Velocity restitution coefficient
$e$	m	Eccentricity
$\Delta_{GAP}(t)$	m	Total gap in the drum support
$\Delta_{GAPX}(t), \Delta_{GAPZ}(t)$	m	Gap projection in X and Z axes
$x(t), z(t)$	m	Displacements of drum support in the X and Z directions
$A_X, A_Z$	m	Amplitudes of support displacements in the X and Z directions
$\Omega_X, \Omega_Z$	rad/s	Angular velocities in the X and Z directions
$F_{FRICX}, F_{FRICZ}$	N	Friction forces in the X and Z axes
$F_{p1p2}, F_{p10p09}$	N	Forces in the cables (cable between points 1 and 2, and points 9 and 10)
$v_{REL}$	m/s	Slip velocity of drum shaft in the support
$r_{SHAFT}$	m	Radius of shaft of drum
$\mu(v_{REL})$	-	Friction coefficient between shaft and support of drum
$\mu_0, \mu_1$	-	Static and dynamic friction coefficients
$k_F, \mu_0, \mu_1, \gamma_V$		Parameters to describe friction coefficients
$m_{O11}$	kg	Total mass of container and spreader
$x_C, y_C, z_C$	m	Coordinates of mass center of total system „Container-Spreader“
$k_{p2p1}$		Stiffness coefficient of cable
$k_{p7p8}$		Stiffness coefficient of cable
$E_{cable}$	Pa	Modulus of elasticity of cable
$A_{cable}$	$m^2$	Cross section area of cable
$L_{cable}$	m	Length of cable
$c_{p2p1}, c_{p7p8}$	Ns/m	Damping coefficient of cable
$L_{p7p8}$	m	Length of cable

$k_{SP}$	N/m	Contact stiffness between container and ship
$\delta_{X,K}$	m	Penetration of k container corner with ship
$\mu(\Delta V_{Y,k}), \mu(\Delta V_{Z,k})$	m	Friction coefficient of k container corner with ship Y and Z direction
$\Delta V_{Y,k}, \Delta V_{Z,k}$	m/s	Slip velocity container corner k in Y and Z directions

The hoist transmission of the crane consists of an asynchronous electric motor, gearbox, and drum (Fig.1 and Fig.2). The dynamic model of drum shaft and support is presented in Fig 3.

Gearbox consists of planetary gear and two-gear join. The gear ratio of transmission is equal:

$$u_R = -\varphi_2 / \varphi_9. \quad (1)$$

Gear ratios of planetary gear, two gear join and total gear ratio are:

$$u_{PL} = 2r_7 / r_2, \quad u_G = r_9 / r_8, \quad u_R = u_{PL}u_G. \quad (2)$$

The reduction mass inertia of crane hoist transmission is equal:

$$I_{2R} = \left( I_2 u_{PL}^2 + I_3 \left( \frac{r_7}{r_3} \right)^2 u_{PL}^2 + (m_1 + m_2 + m_3) r_7^2 u_{PL}^2 + (I_7 + I_8) u_{PL}^2 + I_9 \right) u_G \quad (3)$$

The mathematical model to evaluate the rotation of the transmission elements is:

$$\dot{M}_{eng} + d_v M_{eng} = c_v (\omega_0 - \dot{\varphi}_1) \quad (4)$$

System of equations of simplified hoist transmission are:

$$I_1 \ddot{\varphi}_1 = M_{eng} - k_{12} (\varphi_1 + u_R \varphi_{2R}) - c_{12} (\dot{\varphi}_1 + u_R \dot{\varphi}_{2R}) \quad (5)$$

$$I_{2R} \ddot{\varphi}_{2R} = -k_{12} u_R (u_R \varphi_{2R} - \varphi_1) - c_{12} u_R (u_R \dot{\varphi}_{2R} - \dot{\varphi}_1) - k_{910} (\varphi_{2R} - \varphi_{10}) - c_{910} (\dot{\varphi}_{2R} - \dot{\varphi}_{10}) - c_2 \dot{\varphi}_{2R} \quad (6)$$

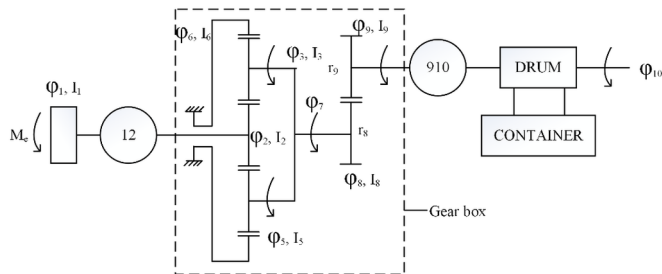


Fig. 1. Hoist transmission of crane

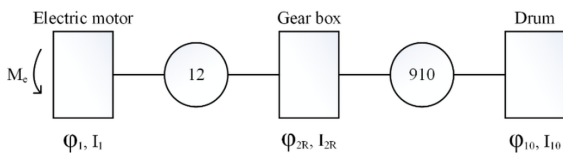


Fig. 2. Simplified hoist transmission of crane

$$m_{O10} \ddot{\varphi}_{O10X} = F_{O10XLR} + F_{O10X} \quad (7)$$

$$m_{O10} \ddot{\varphi}_{O10Z} = F_{O10ZRL} + F_{O10Z}, \quad (8)$$

$$I_{10} \ddot{\varphi}_{10} = -k_{910} (\varphi_{10} - \varphi_{2R}) - c_{910} (\dot{\varphi}_{10} - \dot{\varphi}_{2R}) - c_{10} \dot{\varphi}_{10} + M_{\varphi_{10}} + M_{\varphi_{10},FRIC} \quad (9)$$

$$M_{\varphi_{10}} = r_{10} (F_{p2p1} + F_{p10p9}) \quad (10)$$

$$F_{O10XRL} = F_{NX} + F_{FRICX} \quad (11)$$

$$F_{NX} = -|F_N| \cos(\alpha) \quad (12)$$

$$F_{O10ZRL} = F_{NZ} + F_{FRICZ} \quad (13)$$

$$F_{NZ} = -|F_N| \sin(\alpha) \quad (14)$$

$$\tan(\alpha) = q_{O10Z} / q_{O10X} \quad (15)$$

$$F_N = k_{SUPP} |\delta_N|^n D(\dot{\delta}_N). \quad (16)$$

$$\delta_N = e - \Delta_{GAP}(t), \quad \dot{\delta}_N = \dot{e} - \dot{\Delta}_{GAP}(t) \quad (17)$$

$$D = (1 + 0.75 * (1 - e_{RES}^2)) \dot{\delta}_N / \dot{\delta}_{N\_max} \quad (18)$$

$$e = \sqrt{q_{O10X}^2 + q_{O10Z}^2} \quad (19)$$

The total gap in the drum support, gap projection in X and Z axes:

$$\Delta_{GAP}(t) = \Delta_{GAPX}(t) \cos(\alpha) + \Delta_{GAPZ}(t) \sin(\alpha) \quad (20)$$

$$\Delta_{GAPX}(t) = \Delta_{GAPX0} - x(t) = \Delta_{GAPX0} - A_X \sin(\Omega_X t) \quad (21)$$

$$\Delta_{GAPZ}(t) = \Delta_{GAPZ0} - z(t) = \Delta_{GAPZ0} - A_Z \sin(\Omega_Z t) \quad (22)$$

$$F_{FRICX} = -F_{FRIC} \sin(\alpha) \text{sign}(v_{REL}) \quad (23)$$

$$F_{FRICZ} = -F_{FRIC} \cos(\alpha) \text{sign}(v_{REL}) \quad (24)$$



$$[\tilde{r}] = \begin{bmatrix} 0 & -(z+z_C) & (y+y_C) \\ (z+z_C) & 0 & -(x+x_C) \\ -(y+y_C) & (x+x_C) & 0 \end{bmatrix} \quad (30)$$

is generated using vector:

$$\{r\}^T = [x+x_C \quad y+y_C \quad z+z_C] \quad (31)$$

here  $x_c, y_c, z_c$  – coordinates of mass center of total system „Container-Spreader“;  $\{a_{011}\}$  – acceleration vector:

$$\{a_{011}\} = [A(\theta_{011})][\tilde{\varphi}_{011}]^2 \{S_{011,C}\} - [A(\theta_{011})][\tilde{S}_{011,C}][\dot{G}_2(\theta_{011})]\{\dot{\theta}_{011}\} \quad (32)$$

$$\{M_{011,\theta}\} = [G_2(\theta_{011})]^T [I_{011}][\dot{G}_2(\theta_{011})]\{\dot{\theta}_{011}\} - [G_2(\theta_{011})]^T [\tilde{\varphi}_{011}][I_{011}]\{\dot{\varphi}_{011}\} \quad (33)$$

here:

$$[G_2] = \begin{bmatrix} \cos(\theta_2)\cos(\theta_3) & \sin(\theta_3) & 0 \\ -\cos(\theta_2)\sin(\theta_3) & \cos(\theta_3) & 0 \\ \sin(\theta_2) & 0 & 1 \end{bmatrix} \quad (34)$$

$\{\dot{\varphi}_{011}\}$  – is vector of angular velocity in the body coordinate system

$$\{\dot{\varphi}_{011}\} = [G_2(\theta_{011})]\{\dot{\theta}_{011}\} \quad (35)$$

$$[\tilde{S}_{011,C}] = \int_V [\tilde{r}] \rho dV, \quad (36)$$

$$\{S_{011,C}\} = \int_V \{r\} \rho dV. \quad (37)$$

If container is symmetrical body, then:

$$[\tilde{S}_{011,C}] = 0, \{S_{011,C}\} = 0. \quad (38)$$

Relation between vector  $\{\dot{\varphi}_{011}\}$  and first derivative of Cardan's angles vector  $\{\dot{\theta}_{011}\}$  equal to:

$$\{\dot{\varphi}_{011}\} = [G_2(\theta_{011})]\{\dot{\theta}_{011}\}. \quad (39)$$

Vector of coordinates and velocity of point  $k$  of container area equal to:

$$\{R\} = \{q_{011}\} + [A(\theta_{011})]\{r_k\}, \quad (40)$$

$$\{V_K\} = \{\dot{q}_{011}\} - [A(\theta_{011})][\tilde{r}_{011,k}][G_2(\theta_{011})]\{\dot{\theta}_{011}\}. \quad (41)$$

The vector of forces and vector of moments between points 1 and 2 is equal:

$$\{F_{q011,p2p1}\} = -\frac{F_{p2p1}}{L_{p2p1}}(\{R_{p1}\} - \{R_{p2}\}), \quad (42)$$

$$\{F_{\theta011,p2p1}\} = -\frac{F_{p2p1}}{L_{p2p1}}([A(\theta_{011})][\tilde{r}_{011,2}][G_2(\theta_{011})])^T (\{R_{p1}\} - \{R_{p2}\}) \quad (43)$$

here:

$$F_{p2p1} = k_{p2p1} \left( |\{R_{p1}\} - \{R_{p2}\}| - L_{p2p1,0} + r_{12}\varphi_{12} - r_{10}\varphi_{10} \right) \times \\ \times c_{p2p1} \left( (\{\dot{R}_{p1}\} - \{\dot{R}_{p2}\})^T (\{R_{p1}\} - \{R_{p2}\}) + r_{12}\dot{\varphi}_{12} - r_{10}\dot{\varphi}_{10} \right) \quad (44)$$

$\{R_{p1}\}, \{R_{p2}\}$  – vectors of points 1 and 2.

$$k_{p2p1} = \frac{E_{cable} A_{cable}}{L_{p2p1}} \quad (45)$$

$$L_{p2p1} = \sqrt{(\{R_{p1}\} - \{R_{p2}\})^T (\{R_{p1}\} - \{R_{p2}\})}, \quad (46)$$

$$\{R_{p1}\} = \{R_{O10,19}\} + \{q_{O10}\}, \quad (47)$$

$$\{R_{p2}\} = \{R_{O11,0}\} + \{q_{O11}\} + [A(\theta_{011})]\{r_{O11,p2}\}, \quad (48)$$

here  $[\tilde{r}_{011,2}]$  – antisymmetric matrix which generates by using vector  $\{r_{011,p2}\}$ . This vector is described in the container coordinate system  $X_{o11}, Y_{o11}$ , and  $Z_{o11}$ . The vector of forces and vector of moments, between points 9 and 10, are equal:

$$\{F_{qO11,p10p9}\} = -\frac{F_{p10p9}}{L_{p10p9}}(\{R_{p9}\} - \{R_{p10}\}), \quad (49)$$

$$\{F_{\theta O11,p10p9}\} = -\frac{F_{p10p9}}{L_{p10p9}}([A(\theta_{011})][\tilde{r}_{011,10}][G_2(\theta_{011})])^T (\{R_{p9}\} - \{R_{p10}\}), \quad (50)$$

The vector of forces and vector of moments between points 7 and 8, is equal:

$$\{F_{qO11,p7p8}\} = -\frac{F_{p7p8}}{L_{p7p8}}(\{R_{p9}\} - \{R_{p7}\}), \quad (51)$$

$$\{F_{\theta O11,p7p8}\} = -\frac{F_{p7p8}}{L_{p7p8}}([A(\theta_{011})][\tilde{r}_{011,7}][G_2(\theta_{011})])^T (\{R_{p8}\} - \{R_{p7}\}), \quad (52)$$

here:

$$F_{p7p8} = k_{p7p8} \left( |\{R_{p8}\} - \{R_{p7}\}| - L_{p7p8,0} - r_{14}\varphi_{14} \right) + \quad (53)$$

$$+ c_{p2p1} \left( (\{\dot{R}_{p1}\} - \{\dot{R}_{p2}\})^T (\{R_{p1}\} - \{R_{p2}\}) - r_{40}\dot{\varphi}_{14} \right), \quad (54)$$

$$k_{p7p8} = \frac{E_{cable} A_{cable}}{L_{p7p8}}, \quad (55)$$

$$L_{p7p8} = \sqrt{\left(\{R_{p8}\} - \{R_{p7}\}\right)^T \left(\{R_{p8}\} - \{R_{p7}\}\right)}, \quad (56)$$

Here  $\{R_{p7}\}$ ,  $\{R_{p8}\}$  – vectors of points 7 and 8,

$$\{R_{p7}\} = \{R_{O11,0}\} + \{q_{O11}\} + [A(\theta_{O11})]\{r_{O11,p7}\}, \quad (57)$$

$[\tilde{r}_{O11,7}]$  – antisymmetric matrix which generates by using vector  $\{r_{O11,p7}\}$ . This vector describes the container coordinate system Xo11, Yo11, and Zo11. The system of rotation equations of discs O12, O13 and O14 are equal to:

$$I_{12}\ddot{\phi}_{12} = -r_{12}F_{p2p1} + k_{34}r_{12}(r_{12}\phi_{12} + r_{13}\phi_{13}) + c_{34}r_{12}(r_{12}\dot{\phi}_{12} + r_{13}\dot{\phi}_{13}) - c_{12}\dot{\phi}_{12}, \quad (58)$$

$$I_{13}\ddot{\phi}_{13} = -k_{34}r_{13}(r_{12}\phi_{12} + r_{13}\phi_{13}) - c_{34}r_{13}(r_{12}\dot{\phi}_{12} + r_{13}\dot{\phi}_{13}) - c_{13}\dot{\phi}_{13} - k_{56}r_{13}(r_{13}\phi_{13} + r_{14}\phi_{14}) - c_{34}r_{13}(r_{13}\dot{\phi}_{13} + r_{14}\dot{\phi}_{14}), \quad (59)$$

$$I_{14}\ddot{\phi}_{14} = r_{14}F_{p7p8} - k_{56}r_{14}(r_{13}\phi_{13} + r_{14}\phi_{14}) + c_{56}r_{14}(r_{13}\dot{\phi}_{13} + r_{14}\dot{\phi}_{14}) - c_{14}\dot{\phi}_{14}. \quad (60)$$

The system of rotation equations of discs O15, O16 and O17 are equal:

$$I_{15}\ddot{\phi}_{15} = -r_{15}F_{p10p9} + k_{1112}r_{15}(r_{15}\phi_{15} + r_{16}\phi_{16}) + c_{1112}r_{15}(r_{15}\dot{\phi}_{15} + r_{16}\dot{\phi}_{16}) - c_{15}\dot{\phi}_{15} \quad (61)$$

$$I_{16}\ddot{\phi}_{16} = -k_{1112}r_{16}(r_{15}\phi_{15} + r_{16}\phi_{16}) + c_{1112}r_{16}(r_{15}\dot{\phi}_{15} + r_{16}\dot{\phi}_{16}) - c_{16}\dot{\phi}_{16} - k_{1314}r_{16}(r_{16}\phi_{16} + r_{17}\phi_{17}), \quad (62)$$

$$I_{17}\ddot{\phi}_{17} = r_{17}F_{p15p16} - k_{1314}r_{17}(r_{16}\phi_{16} + r_{17}\phi_{17}) + c_{1314}r_{17}(r_{16}\dot{\phi}_{16} + r_{17}\dot{\phi}_{17}) - c_{17}\dot{\phi}_{17}, \quad (63)$$

here force  $F_{p10p9}$  is described the same as force  $F_{p2p1}$  and force  $F_{p15p16}$  is described the same as force  $F_{p7p8}$ .

The container is unloading from the ship hold in the form of a rectangular parallelepiped. The node  $k$  global vector coordinates and velocities of rectangular parallelepiped are equal:

$$\{R_{SK}\} = \{R_{OS}\} + \{R_{OS,K}\} + \{q_s(t)\}, \quad (64)$$

$$\{V_{SK}\} = \{\dot{q}_s(t)\}, \quad (65)$$

here  $\{R_{OS}\}$  - initial vector coordinates of rectangular parallelepiped center;  $\{R_{OS,K}\}$  – vector from point OS to angle  $k$  of rectangular parallelepiped;  $\{q_s(t)\}$  – vector coordinates of rectangular parallelepiped center:

$$\{q_s(t)\}^T = [A_X \sin(\Omega_X t) A_Y \sin(\Omega_Y t) A_Z \sin(\Omega_Z t)]. \quad (66)$$

The node  $k$  global vector coordinates and velocities of container corners are equal:

$$\{R_K\} = \{R_{O11,0}\} + \{q_{O11}\} + [A(\theta_{O11})]\{r_{O11,K}\}, \quad (67)$$

$$\{V_K\} = \{\dot{q}_{O11}\} - [A(\theta_{O11})][\tilde{r}_{O11,K}][G_2(\theta_{O11})]\{\dot{\theta}_{O11}\}, \quad (68)$$

Here  $\{r_{O11,K}\}$  – vector of coordinates of corner  $k$ , ( $k = 1, 2, \dots, 8$ ). Initial gaps of container corner and ship rectangular parallelepiped corner in the X, Y, Z directions are equal:

$$\{\Delta\}^T = [\Delta_X \quad \Delta_Y \quad \Delta_Z]. \quad (69)$$

Contact forces between container and ship are described in eight angles of container (Fig.5). The normal contact force in the X direction of  $k$  container corner with ship rectangular parallelepiped corner  $k$  is equal:

$$F_{NX,K} = k_{SC} |\delta_{X,K}|^n D(\delta_{X,K}), \quad (70)$$

$$\delta_{X,K} = \begin{cases} X_{SK} - X_K - \Delta_{SCX}, & \text{when } k = 1, 4, 5, 8 \\ X_K - X_{SK} - \Delta_{SCX}, & \text{when } k = 2, 3, 6, 7 \end{cases} \quad (71)$$

$$\dot{\delta}_{X,K} = \begin{cases} V_{SKX} - V_{KX}, & \text{when } k = 1, 4, 5, 8 \\ V_{KX} - V_{SKX}, & \text{when } k = 2, 3, 6, 7 \end{cases} \quad (72)$$

$D$  – coefficient which evaluates hysteresis of contact force:

$$D = (1 + 0.75 * (1 - e^{2\delta_{RES}})) \dot{\delta}_{NX} / \dot{\delta}_{N\_max}. \quad (73)$$

The friction forces in the Y and Z directions are equal:

$$F_{Y,K,FRIC} = -\mu(\Delta V_{Y,K}) F_{NX,K} \text{sign}(\Delta V_{Y,K}), \quad (74)$$

$$F_{Z,K,FRIC} = -\mu(\Delta V_{Z,K}) F_{NX,K} \text{sign}(\Delta V_{Z,K}), \quad (75)$$

slip velocities are equal:

$$\Delta V_{Y,K} = V_{Y,K} - V_{SY,K}, \Delta V_{Z,K} = V_{Z,K} - V_{SZ,K}. \quad (76)$$

The total force and moment vector of container corner  $k$  with ship is equal:

$$\{M_K\} = -[G_2(\theta_{O11})]^T [\tilde{r}_{O11,K}]^T [A(\theta_{O11})]^T \{F_K\} \quad (77)$$

The contact forces in the Y and Z axis directions are similarly determined.

#### 4. Experimental results of container loading process

Experimental measurements of the container loading process in the port were done. During the experimental research, the quay crane carried out loading operations. Main parameters of the container unloading process were measured: duration (s), position X, Y, Z (m), velocity (m/s) acceleration (m/s<sup>2</sup>). Data was collected using equipment “DL1-MK2 data logger” which was fixed on a spreader of a crane. More than 200 of container unloading processes were measured and statistical analysis of data was performed. More detail information about experimental measurements is presented in the paper [7]. Measurement results of the unloading process were divided into operations

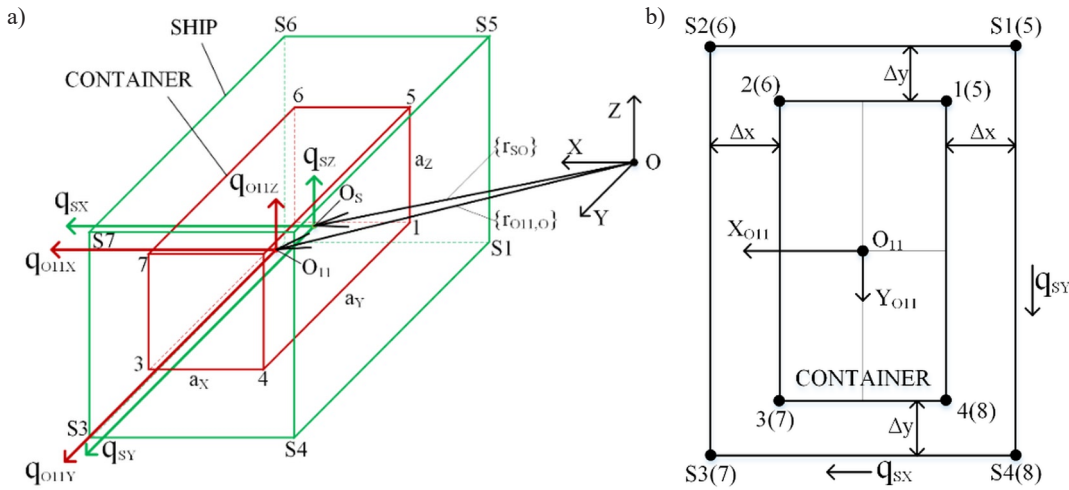


Fig. 5. The container corners and ship rectangular parallelepiped corners: red color–container; green color–ship rectangular parallelepiped

of 7 stages: 1. Start of lifting (hooking); 2. Vertical lifting; 3. Diagonal lifting; 4. Horizontal transportation; 5. Diagonal lowering; 6. Vertical lowering; 7. Placing on (autonomous guided vehicle) AGV.

The data that is relevant for the analysis of unloading containers from the ship: mass of the container, duration of hooking, time of vertical lifting from the ship. The results of the experimental unloading duration are presented in Fig. 6.

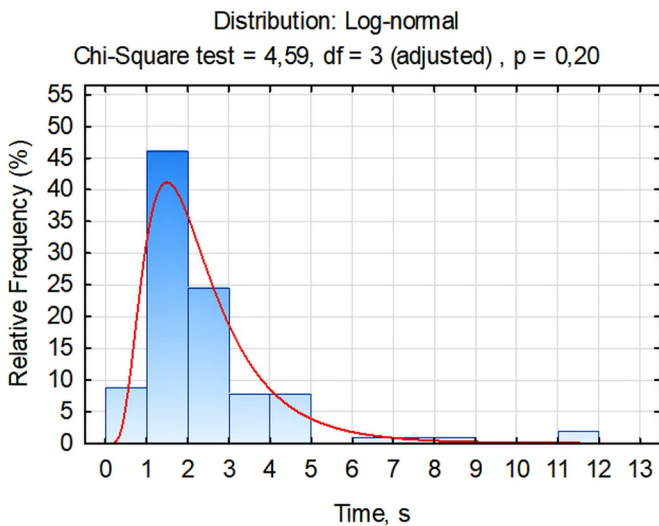


Fig. 6. The duration of hooking the container

The hooking duration of the container on the ship can vary from 0,6 to 12 (s), average is 2,43 (s). Results of the vertical lifting duration from the ship cargo hold are shown in Fig. 7.

The duration of the vertical lifting from the ship depends on the depth at which the container is located; coefficient of correlation is equal  $r=0,89$ .

Histogram of container masses is presented in Fig 8. The needs of power for the unloading process depends on the mass of the container, which can vary. Analysis of container masses shows that masses can vary from 2 to 32 tons.

As we can see from the histogram, more than 67 % of container masses are from 25 to 32 tons.

Results of experimental measurements were used to compare the results of mathematical model and numerical analysis with the real data of container unloading from the ship. More results of measurements (acceleration, velocity, displacement) are presented in section 5 Figures 9b, 10b, 11b.

## 5. Results of numerical analysis

Based on the mathematical model presented in section 2 the computer programming code was created and numerical analysis of container unloading from the ship's cargo hold was performed. Time step for integration of differential equations was  $10^{-6}$  s. The main parameters of the system are given in Table 2.

Numerical analysis was performed when the gap between container and ship's hold wall varies from 10 mm to 50 mm.

Results of numerical modeling are shown in Figures

Table 2. Main parameters used in dynamic model

Symbol	Description [units]	Values
$a_1$	m	1,0
$a_2$	m	1,0
$b_1$	m	0,719
$B_2$	m	0,719
$h_1$	m	1,1
$h_2$	m	0,30
$h_3$	m	1,0
Length of container	m	6,058
Width of container	m	2,438
Hight of container	m	2,60
Depth of hold	m	10
Parameters of electrical motor:		
$I_1$	kgm <sup>2</sup>	1,811
$w_0$	rad/s	78,83
$c_v$	Nm	5093,9
$d_v$	1/s	405,3
$U_R$	-	8,0
$k_{12}$	MNm	0,1636
$c_{12}$	kNms	10,0
$k_{910}$	MNm	0,170
$c_{910}$	kNms	10,0
$d_{cable}$	m	0,30
$E_{cable}$	GPa	
$c_{cable}$	kNs/m	20,0
$r_{10}$	m	20,0
$m_{10}$	kg	20
$I_{10}$	Kgm <sup>2</sup>	0,20
$r_{12}=r_{13}=r_{14}=r_{15}=r_{16}=r_{17}$	m	1973,0
$m_{grapper}$	kg	300,0
$k_{sc}$	GNm <sup>1,5</sup>	1,50
$c_{sc}$	Ns/m	1,0
$e_{RES}$		0,50
$n$	-	1,5

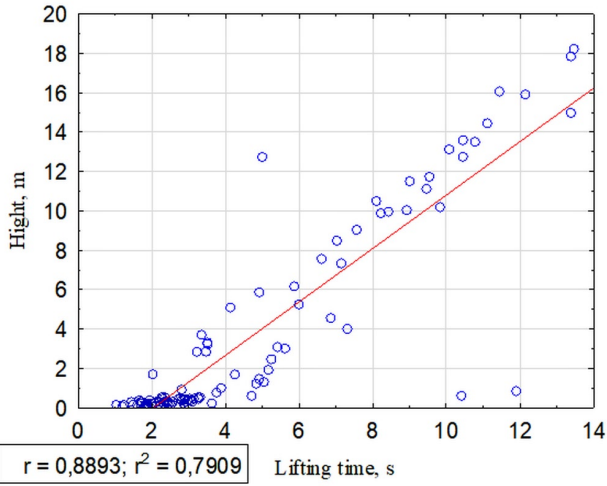


Fig. 7. Relationship between hight and lifting time: experimental measurements

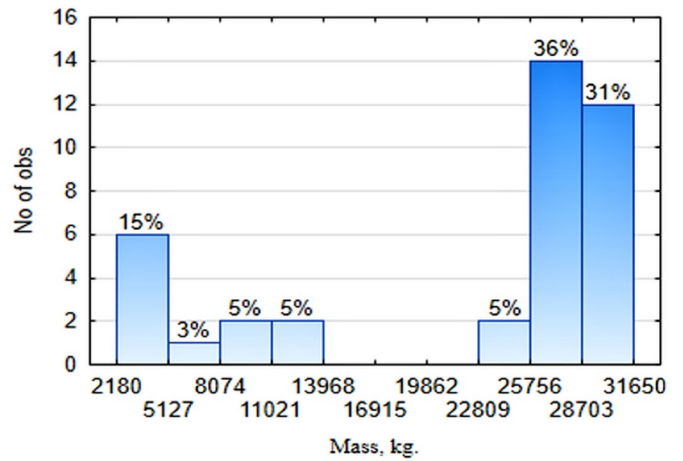


Fig. 8. Container mass distribution

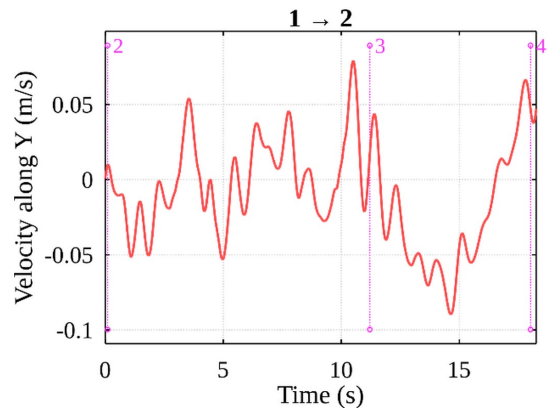
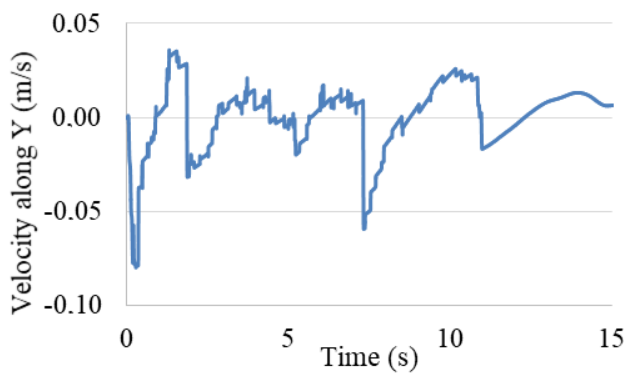


Fig. 9. Cargo movement speed in ship's cargo hold (direction Y): a) mathematical model, b) results of experimental measurements

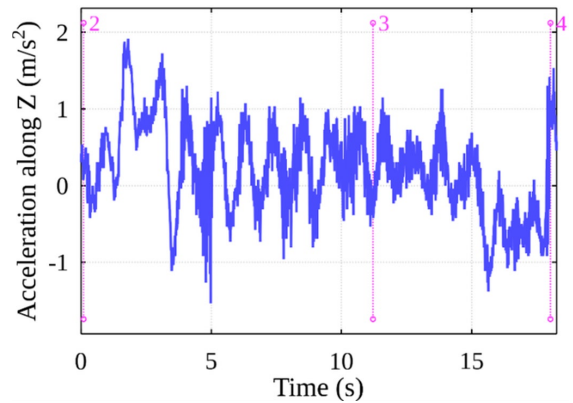
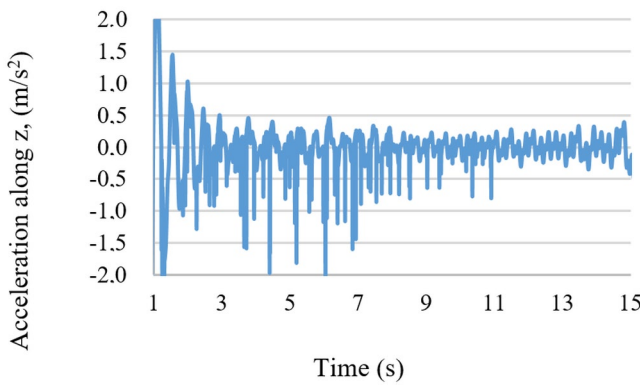


Fig. 10. Lifting acceleration in Z direction: a) mathematical model, b) results of experimental measurements

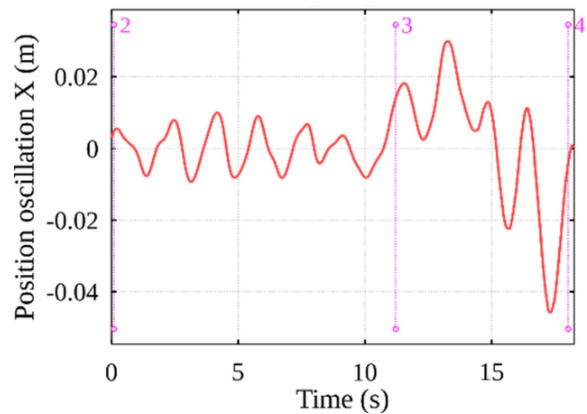
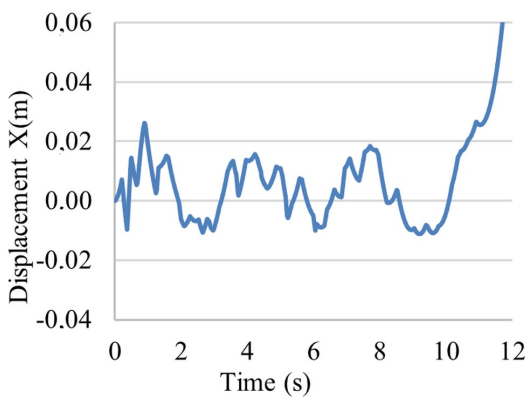


Fig. 11. Container displacements in X direction when loading vertically: a) modelling results, b) results of experimental measurements

9–11, and the obtained results are compared with the results of experimental measurements in case the cargo weight is 28 tons. The velocity of container movement in Y direction is presented in Fig. 9.

As we can see, results of numerical analysis and experimental measurement are very similar i.e., velocity of container movement along Y axis can vary in range  $\pm 0,08$  m/s.

The acceleration in Z direction when the lifted cargo weight is 28 tons is presented in Fig. 10.

We can see that acceleration can vary in range from  $-2$  m/s<sup>2</sup> to  $+2$  m/s<sup>2</sup> during experimental measurement and results of numerical analysis.

Container displacements in X direction are shown in Fig. 11. Results show that container displacements in the ship's cargo hold can be approximately  $\pm 0.02$ m. When the cargo is lifted at about the 11th second, container displacement along the X-axis can increase because it is not limited by ship hold and can move freely. This dependence we can see both during numerical analysis and during the real unloading process.

The power of friction forces when there are oscillations of the ship and contact forces are taken into consideration is presented in Fig. 12.

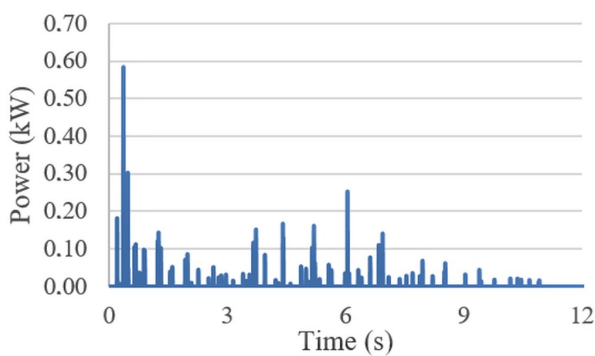


Fig. 12. Power of friction forces

We can see in Fig. 12 if the ship starts to oscillate and cargo comes into contact with the ship's cargo hold wall, then arises the need for additional power.

Mathematical modelling results of power needs of cargo lifting are presented in Fig. 13. We can see dependency power from cargo mass, approximately 220 kW power needed to lift cargo with mass 32 t.

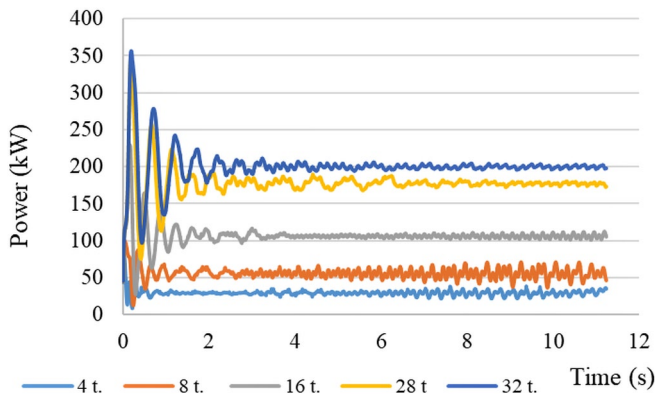


Fig. 13. Lifting power dependency from container mass

Power needs depending on friction forces between container and ship's cargo hold when the ship's oscillating toward X direction was calculated. Results of power of friction forces when the gap is  $10 \pm 50$  mm and frequency of ship oscillation is 0,30 Hz are shown in Table 3.

Table 3. Power of friction forces depending on cargo masses

Cargo mass, tons	Gap, mm	Average power of friction forces, kW
4,0	10	0,433
8,0	10	1,024
24,0	10	1,343
28,0	10	1,506
28,0	30	1,532
28,0	50	2,121

From the given average power of friction force we can see that the power of friction force increases when the cargo mass increases. However, this dependency is nonlinear because the contact forces depend on container mass and mass inertia moments, ship's oscillation, lifting speed, varying rope stiffness, dynamic characteristics of drum bearings.

## 5. Discussion and conclusions

Mathematical model and programming code were created that allows to determine main parameters of container lifting from ship process: container displacement, velocity, acceleration in X, Y, Z directions during cargo loading process when container movement is limited in the cargo hold in X, Y directions.

Results of experimental measurements of the container unloading process are used for verification of mathematical models and show similar results as numerical analysis.

Mathematical model considers friction forces that occur during the container contact with the ship cargo hold.

Based on real time container loading results it was determined that containers on the ship can be hooked within  $0,6 \div 11,5$  (s), the average of hooking time being  $2,43 \pm 1,84$  (s).

Experimental measurements of container unloading *in situ* showed that usually container mass is between 24 and 32 tons. Small mass containers (less than 4 tons) make up 15% of all containers. Duration of vertical unloading depends on the weight of the cargo; however, this dependency is not very significant. Mass has a greater impact on energy consumption. Results of modelling show that power consumption during unloading has a nonlinear dependency from cargo mass. The power depends on container mass and 32 tons cargo requires about 220 kW power.

Low oscillations of the ship affect the stability of the container unloading process and power consumption. Contact of container to ship hold can cause frictional forces and increase instantaneous power requirements. The results of mathematical modelling show if the container has a contact with the cargo hold and the ship's oscillation frequency is 0,3Hz, then average power of friction forces increases and is equal to about 2,12 kW.

As we can see from the analysis of frictional power, this power is useless and reduces the energy efficiency of the system. This energy can be saved by controlling the lifting gear using special methods and smart technologies.

Based on results further research of cargo unloading from ships can be continued and rational unloading modes determined to minimize energy consumption and avoid possible cargo damage from contact forces.

### Acknowledgements

The authors express gratitude to members of the project No. 01.2.2-LMT-K-718-01-0081: Dr R. Didziokas, Dr A. Senulis, Dr T. Eglynas, Dr. S.Jakovlev, Z Lukosius for valuable insights and collection of data.

### Funding

The author(s) disclosed receipt of the following financial support for the research, authorship, and/or publication of this article: This research was funded by the European Regional Development Fund according to the supported activity "Research Projects Implemented by World-class Researcher Groups" under Measure No. 01.2.2-LMT-K-718-01-0081.

### References

1. Abdullahi A M, Mohamed Z, Selamat H, Pota H R, Zainal Abidin M S, Fasih S M. Efficient control of a 3D overhead crane with simultaneous payload hoisting and wind disturbance: design, simulation and experiment. *Mechanical Systems and Signal Processing* 2020; 145: 106893, <https://doi.org/10.1016/j.ymssp.2020.106893>.
2. Alamouh A S, Ballini F, Ölçer AI. Ports' technical and operational measures to reduce greenhouse gas emission and improve energy efficiency: A review. *Marine Pollution Bulletin* 2020; 160: 111508, <https://doi.org/10.1016/j.marpolbul.2020.111508>.
3. Arena A, Casalotti A, Lacarbonara W, Cartmell M P. Dynamics of container cranes: three-dimensional modeling, full-scale experiments, and identification. *International Journal of Mechanical Sciences* 2015; 93: 8-21, <https://doi.org/10.1016/j.ijmecsci.2014.11.024>.
4. Bouman E A, Lindstad E, Rialland A I, Strømman A H. State-of-the-art technologies, measures, and potential for reducing GHG emissions from shipping - A review. *Transportation Research Part D: Transport and Environment* 2017; 52 (A): 408-421, <https://doi.org/10.1016/j.trd.2017.03.022>.
5. Çağatay I, Lam J S L. A review of energy efficiency in ports: Operational strategies, technologies and energy management systems. *Renewable and Sustainable Energy Reviews* 2019; 112: 170-182, <https://doi.org/10.1016/j.rser.2019.04.069>.
6. Chu Y, Li G, Hatledal L I, Holmeset F T, Zhang H. Coupling of dynamic reaction forces of a heavy load crane and ship motion responses in waves. *Ships and Offshore structures* 2021; 16(1): 58-67, <https://doi.org/10.1080/17445302.2021.1907066>.
7. Chwastek S. Optimization of crane mechanisms to reduce vibration. *Automation in Construction*, 2020; 119(1): 103335, <https://doi.org/10.1016/j.autcon.2020.103335>.
8. Eglynas T, Andziulis A, Bogdevicius M, Januteniene J, Jakovlev S, Jankunas V, Senulis A, Jusis M, Bogdevicius P, Gudas S. Modeling and experimental research of quay crane cargo lowering processes. *Advances in Mechanical Engineering* 2019; 11(12), <https://doi.org/10.1177/1687814019896927>.
9. European Sea Ports Organization. ESPO Green Guide 2021 A Manual for European Ports Towards A Green Future 2021.
10. Hoang M C, Hoang Q D, Pham V T, Le A T. Adaptive fractional-order terminal sliding mode control of rubber-tired gantry cranes with uncertainties and unknown disturbances. *Mechanical Systems and Signal Processing* 2021; 154: 107601, <https://doi.org/10.1016/j.ymssp.2020.107601>.
11. Jakovlev S, Eglynas T, Voznak M. Application of Neural Network Predictive Control Methods to Solve the Shipping Container Sway Control Problem in Quay Cranes. *IEEE Access* 2021; PP(99):1-1, <https://doi.org/10.1109/ACCESS.2021.3083928>.
12. Kosucki A, Malenta P, Stawiński L, Halusia S. Energy consumption and overloads of crane hoisting mechanism with system of reducing operational loads. *Eksploatacja i Niezawodność - Maintenance and Reliability* 2017; 19(4): 508-515, <https://doi.org/10.17531/ein.2017.4.3>.
13. Kosucki A, Stawiński L, Malenta P, Zaczyński J, Skowroński J. Energy consumption and energy efficiency improvement of overhead crane's mechanisms. *Eksploatacja i Niezawodność - Maintenance and Reliability* 2020; 22(2): 323-330, <https://doi.org/10.17531/ein.2020.2.15>.
14. Merk O. Shipping Emissions in Ports. *International Transport Forum, Paris, France* 2014; Paper No. 2014-20.
15. Milana G, Banisoleiman K, González A. An investigation into the moving load problem for the lifting boom of a ship unloader. *Engineering Structures* 2021; 234: 111899, <https://doi.org/10.1016/j.engstruct.2021.111899>.
16. Papaioannou V, Pietrosanti S, Holderbaum W, Becerra V M, Mayer R. Analysis of energy usage for RTG cranes. *Mechanical Systems and Signal Processing* 2018; 125: 337-344, <https://doi.org/10.1016/j.energy.2017.02.122>.
17. Phan-Thi M, Ryu K, Kim K H. Comparing Cycle Times of Advanced Quay Cranes in Container Terminals. *Industrial Engineering & Management Systems* 2013; 12(4): 359-367, <https://doi.org/10.7232/iems.2013.12.4.359>.
18. Sun N., Wu Y., He Chen, Fang Y. An energy-optimal solution for transportation control of cranes with double pendulum dynamics: Design and experiments. *Mechanical Systems and Signal Processing* 2018; 102: 87-101, <https://doi.org/10.1016/j.ymssp.2017.09.027>.
19. Urbaś A, Szczotka M. The influence of the friction phenomenon on a forest crane operator's level of discomfort. *Eksploatacja i Niezawodność - Maintenance and Reliability* 2019; 21(2): 197-210, <https://doi.org/10.17531/ein.2019.2.3>.
20. Wu Q, Wang X, Hua L, Xia M. Improved time optimal anti-swing control system based on low-pass filter for double pendulum crane system with distributed mass beam. *Mechanical Systems and Signal Processing* 2021; 151(9): 107444, <https://doi.org/10.1016/j.ymssp.2020.107444>.
21. Wu Q, Wang X, Hua L, Xia M. Modelling and nonlinear sliding mode controls of double pendulum cranes considering distributed mass beams, varying roped length and external disturbances. *Mechanical Systems and Signal Processing* 2021; 158: 107756, <https://doi.org/10.1016/j.ymssp.2021.107756>.
22. Yurchenko D, Alevras P. Stability, control and reliability of a ship crane payload motion. *Probabilistic Engineering Mechanics* 2014; 38: 173-179, <https://doi.org/10.1016/j.probenmech.2014.10.003>.